JOURNAL OF CATALYSIS 152, 322–330 (1995)

Characterization of Gold(I) in NaY Zeolite and Acidity Generation

Tarek M. Salama,[1] Takafumi Shido, Hideki Minagawa, and Masaru Ichikawa[2]

Catalysis Research Center, Hokkaido University, Sapporo 060, Japan

Received June 13, 1994; revised October 24, 1994

Au(I) ions were incorporated into NaY zeolite via solid–vapor reaction between Au_2Cl_6 vapor and partially dehydrated zeolite in high vacuum. The process involved the evolution of HCl, as monitored by temperature-programmed desorption–mass, resulting in the reduction of Au(III) into Au(I). X-ray photoelectron spectroscopy characterization of Au^{n+}/NaY revealed the Au $4f_{7/2}$ peak exhibited a chemical shift by +1.95 eV relative to that of Au^0, implying the formation of surface AuCl or like species. Upon the introduction of Au_2Cl_6 into NaY zeolite, the IR OH band at 3690 cm^{-1} due to cation–water interaction in NaY zeolite declined. On the other hand, a strong hydroxyl band at 3640 cm^{-1} was delivered due to polarization of H_2O in zeolite by the electrostatic potential associated with the Au^{n+} ($n > 1$) ions. Adsorption of D_2O onto Au_2Cl_6/NaY at room temperature produced a peak at 2656 cm^{-1} due to OD species associated with Au^{n+} ($n > 1$). Degassing of D_2O at 333 K reduced this peak in favor of a new band at 2690 cm^{-1} which is assigned to O–D stretching mode in the Au (OD)Cl moiety. The CO chemisorption onto Au(I)/NaY at 77 K followed by evacuation to reduced pressures showed a unique carbonyl band at 2188 cm^{-1}, which is characteristic of Au(I) ions. The evolution of HCl during the solid–vapor reaction produced protonic sites, which were detected by Fourier transform infrared of pyridine adsorption. The concentration of these sites increased up to 353 K, where the solid–vapor reaction leveled off. The subsequent pyridine–Cl_2 adsorption did not lead to changes in the oxidation state of Au(I) ions, indicating that NaY zeolite stabilized their structure.

INTRODUCTION

The chemistry of gold and its compounds still receives considerable attention. Part of this interest is caused by a number of investigations of the catalytic behavior and properties of gold (1–4). In these papers, the preparation of active gold catalysts was restricted to the dispersion of gold phase on conventional supports like Al_2O_3, SiO_2, and TiO_2. Since the sublimation energy of gold is low, it is likely to segregate during application of high temperatures. The gold surface morphological changes at high temperatures led to gold's low catalytic performance as an oxidative catalyst (5). Additionally, gold is generally a poor catalyst due to its weak interaction with H_2, CO, and NO. The low catalytic activity of gold has been attributed to its lack of a partially filled *d*-orbital, though a feature necessary for gold catalysts is the prerequisite of a coordinatively unsaturated gold center or active site. Thus, our crucial goal is the introduction and characterization of gold ions inside the NaY zeolite cages.

The solid–vapor reaction is assumed to be more efficient than ion exchange from an aqueous solution of a cation salt (6). In aqueous solution, the ingoing cation is strongly hydrated and prevented by its hydration shell from penetrating into small cavities and channels of the zeolite structure. It was shown that in several cases a one-step solid–vapor reaction leads to a 100% cation incorporation, whereas such a high degree of exchange is difficult to obtain by conventional methods. If one briefly surveys the field of solid–vapor chemistry, one sees that it involves transporting the solid vapor to where it is arranged to react with another material (or solute) to form the desired product (7).

Taking the above considerations into account, we attempted to prepare and characterize a novel gold(I) species inside NaY zeolite to retain its thermal stability and activity. To the best of our knowledge, the characterization of Au(I)/zeolite has not been reported in the literature until now, although we recently reported its virtual effect on NO catalytic decomposition and NO + CO reactions (8–10). The dispersion state of gold was characterized by the X-ray diffraction, the oxidation state and surface composition by X-ray photoelectron spectroscopy (XPS), the catalyst structure and extent of Au_2Cl_6 vapor deposition by Fourier transform infrared (FT-IR) spectroscopy, and the gases desorbed during reaction between Au_2Cl_6 and NaY by temperature-programmed desorption (TPD)–mass.

EXPERIMENTAL

Au(I)/NaY (13 Au wt.%) was prepared at room temperature by careful hand grinding of Au_2Cl_6 (Strem Chemicals, 99% purity) with partially dehydrated NaY

[1] On leave from Chemistry Department, Faculty of Science, Al-Azhar University, Cairo, Egypt.

[2] To whom correspondence should be addressed.

0021-9517/95 $6.00

(Si/Al = 5.6) at 523 K, under nitrogen atmosphere. The Au_2Cl_6/NaY sample was heated to the desired temperature at a ramping rate of 0.2 K min^{-1} in high vacuum (10^{-6} Torr). The steady Au_2Cl_6/NaY reaction was conducted at three temperatures, namely at 328, 338, and 353 K for 72 h, and the samples were referred to as Au(I)/NaY-L, -M, and -H, respectively. The dispersion state of gold cations as a function of reaction time and temperature was followed systematically by X-ray diffraction (XRD) analysis.

XRD spectra of the catalysts were measured on an XRD diffractometer MXP-3 (MAC Science Co., Ltd.) by using Ni-filtered Cu$K\alpha$ radiation. The samples were prepared under nitrogen atmosphere by mixing with drops of liquid paraffin in order to isolate them from their surroundings during handling for measurements. A portion of the thus-prepared paste was mounted on a glass slide for measurement.

FT-IR spectra of 2 Torr pyridine, 15 Torr Cl_2, and 10 μmol H_2O (1 Torr = 133.3 N m^{-1}) adsorptions were carried out in a closed-circulation system with a dead volume of 159 cm^3. An IR cell equipped with NaCl windows was used for both treatments and measurements. A self-supported wafer (20 mg) was prepared under N_2 atmosphere and mounted to the sample holder in the IR cell. The wafer was evacuated at 400 K for 30 min before pyridine adsorption at room temperature. *In situ* CO (0.5 Torr) adsorption at 77 K was carried out in a special cell. The IR spectra were recorded with a resolution of 2 cm^{-1} using a Shimadzu FTIR 8100.

XPS was carried out using ESCA3-MK2 (VG Co.). The apparatus consists of an analysis chamber and a sample preparation chamber (11). Heat treatment and CO adsorption were performed in the preparation chamber under the base pressure of 1×10^{-8} Torr. After each treatment the sample was analyzed in the analysis chamber. For XPS measurements, Mg$K\alpha$ radiation with an energy of 1253.6 eV was used for composition and binding state analysis.

A TPD experiment was conducted in a fixed-bed reactor using 50 mg of fresh Au_2Cl_6/NaY sample. The temperature increased linearly at a rate of 5 K/min. The background pressure was maintained at 3×10^{-7} Torr before starting. The desorbed gases were analyzed by an ANELVA AQA-100 quadrupole spectrometer at an ionization voltage of 50 eV.

RESULTS AND DISCUSSION

Because all the treatments were performed in a quartz reactor, it was possible to monitor the color changes of the samples. The pale yellow color of the Au(I)/NaY-L and -M samples is assumed to be that of NaY zeolite-entrapped Au(I) ions. The color turns reddish-brown for Au(I)/NaY-H.

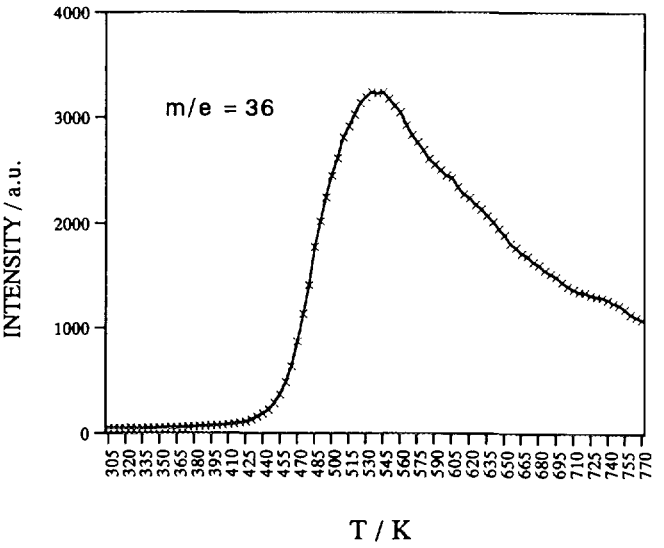

FIG. 1. TPD spectrum of HCl (36 mass) from Au_2Cl_6/NaY.

XRD and TPD Studies of Au^{n+}/NaY Catalysts

X-ray diffraction patterns recorded in the course of these experiments demonstrated that the NaY zeolite structure was fully retained. The unpromoted Au_2Cl_6 was represented by the intense reflections at 2θ = 12.42°, 14.74°, 15.48°, 19.40°, 24.36°, 24.90°, and 25.26°. The XRD spectrum of the Au_2Cl_6/NaY sample after mixing shortly exhibited Au_2Cl_6 weak crystalline lines at 2θ = 12.42° and 14.74°, while the other lines disappears. This result shows that the greater part of the separated Au_2Cl_6 crystallites on the zeolite surface were homogeneously distributed at room temperature. The overall XRD characteristics of the Au(I)/NaY-M sample were similar to those of the NaY zeolite, with a slight feature of Au^0 phase at 2θ = 38.18° and 44.39°. The XRD lines of gold phase had greater intensities in the Au(I)/NaY-H spectrum.

The gases that evolved during the Au_2Cl_6/NaY reaction were monitored by TPD–mass (Fig. 1). The Cl_2 desorption was not evident. On the other hand, a large amount of HCl (m/e = 36) started to desorb around 410 K and continued over a long range of temperatures, with a maximum at 530 K. The evolution of HCl is due to hydrolysis of Au_2Cl_6 by trace of H_2O in zeolite. The HCl desorption temperature was higher than the temperatures at which the Au_2Cl_6/NaY reaction was conducted, suggesting the existence of a strong interaction between HCl and NaY zeolite.

XPS Study

Additional insight into the nature and oxidation states of Au and Cl species in Au_2Cl_6/NaY and Au(I)/NaY-M was provided by XPS. The binding energy (BE) values

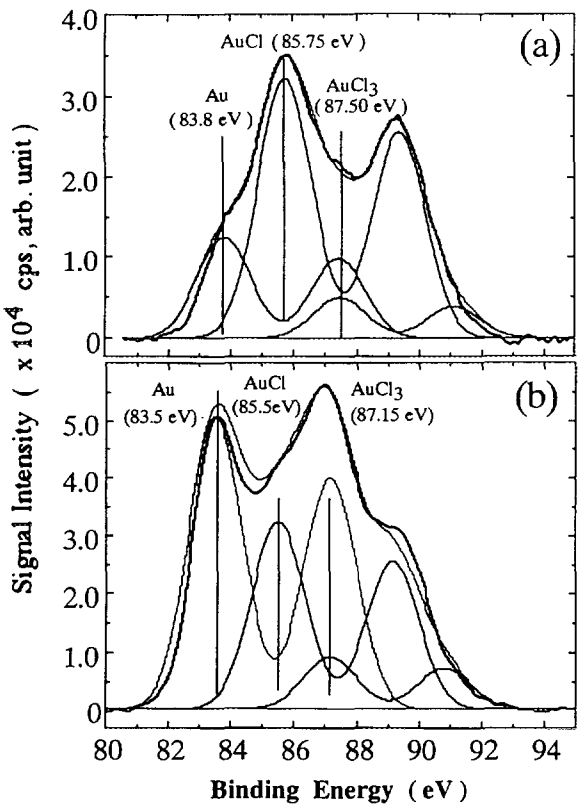

FIG. 2. Deconvoluted 4*f* XPS spectra of (a) Au(I)/NaY-M and (b) (a) after CO (0.5 Torr) adsorption at 373 K.

have been corrected by assuming the Si (2*p*) peak to have a BE of 103.4 eV. Shown in Fig. 2 are the Au (4*f*) XPS spectra of Au(I)/NaY-M before and after CO treatment at 363 K. Each spectrum was deconvoluted by nonlinear least-squares algorithms in order to deduce precise binding energies. Using the peak areas of Au (4*f*) and Cl (2*p*) and employing the relevant elemental sensitivity factor (4.95 for Au (4*f*) and 0.73 for Cl (2*p*)) (12), the $(Cl/Au)_{surface}$ values vary over the range 0.57–2.70. The corrected binding energies of Au^{n+} ($0 \leq n \leq 3$) and the corresponding corrected $(Cl/Au)_{surface}$ values are summarized in Table 1.

TABLE 1

XPS Results of Au^{n+} Entrapped in NaY

	Binding energy (eV)				
	Au $4f_{7/2}$				
Catalyst	Au^0	Au^+	Au^{3+}	Cl 2*p*	Cl 2*p*/Au $4f_{7/2}$
Au_2Cl_6/NaY	—	—	87.7	199	2.70
Au(I)/NaY-M	83.8	85.6	87.5	200.1	0.57
+CO at 373 K	83.5	85.5	87.2	200.4	1.28

Au(III)Cl has a BE shift of +3.5 eV relative to that of Au^0, whereas a BE shift of 2.0 eV has been assumed for Au(I)Cl (13). The Au $4f_{(7/2)}$ BE at 85.75 is shifted by +1.95 eV relative to that of Au metal (Table 1). This chemical shift corresponds to the reduction of surface Au(III)Cl into Au(I)Cl (13). Figure 2 clearly shows that Au(I) indeed was the dominant oxidation state of gold within the probing depth of the photoelectrons. There are also contributions from Au^0 and Au(III) states.

Upon CO (0.5 Torr) admittance onto the Au(I)/NaY-M catalyst at 373 K followed by the evacuation at the same temperature, the Au^0 4*f* peaks were greatly enhanced in intensity. The Au(I) and Au(III) peaks were also enhanced but to a much lesser extent. From the shift in 4*f* lines of Au^{n+} ($0 \leq n \leq 3$) toward lower BE after CO chemisorption (Table 1), it can be argued that such a shift is eventually due to the presence of a small fraction of Au^{n+} species after these treatments. We have suggested that CO interacted with Au(I)Cl to form chlorocarbonyl species bound to Au (IR band at 2188 cm^{-1}) and with Au(III)Cl to form the same species via the reductive carbonylation reaction (8)

$$AuCl_3/NaY + 2CO + H_2O \rightarrow AuCl(CO)/NaY + CO_2 + 2HCl. \quad [1]$$

Anhydrous conditions are necessary for AuCl(CO) species to be stable, possibly due to the decomposition to Au^0, Au(I)Cl, and CO by the reaction with water (14). Since the atomic surface composition of Au^{n+} ($0 \leq n \leq 3$) was increased entirely by CO chemisorption (Fig. 2b), the migration of AuCl(CO) species from cages/channels of NaY zeolite to the surface cannot be excluded. This leads to the assumption that $AuCl_n$ species were built up inside the zeolite cages and channels while the steady-state thermal Au_2Cl_6/NaY reaction was conducted for 72 h. However, the AuCl(CO) species underwent dissociation upon reaction with a trace of water to Au^0 and Au(I)Cl (15). Au(I)Cl is metastable and slowly disproportionate to Au(III)Cl and Au^0 (16, 17).

The observed Cl (2*p*) BE at 200.1 eV for the Au(I)/NaY-M catalyst is much higher than that for the terminal Cl atoms in $KAuCl_4$ (198.10 eV), indicating the bridged Au–Cl–Au structure prevails over the former since a less negative charge on the bridged Cl atoms is expected (18). This observation revealed a pronounced involvement of terminal Cl atoms rather than bridged Cl atom in the reduction process. It was shown that the structure of Au(I)Cl is polymeric with zig-zag chains of Au and Cl atoms, with each Cl bridging between two Au atoms (19, 20).

The stoichiometry Cl/Au of dimer Au_2Cl_6 is 3 and was detected to be less by 0.3 for Au_2Cl_6/NaY. This observation, parallel with the observed higher Cl (2*p*) BE for this

sample relative to the corresponding $KAuCl_4$, indicates that a fraction of the Au cations was reduced during grinding of the Au_2Cl_6–zeolite mixture at room temperature. The picture that emerged from the XRD investigation of Au_2Cl_6/NaY, that Au(III)Cl phase almost disappeared, may confirm this conclusion. The Cl/Au intensity ratio for Au(I)/NaY-M decreased to 0.57, indicating that Cl atoms in Au(III)Cl were reduced to Au(I)Cl and Au^0 on zeolite. This value is less than that expected for the stoichiometric reduction of Au(III)Cl into Au(I)Cl zig-zag structure, i.e., 2, after taking into account the conclusive reduction of Au(III) into Au^0. This may be due to the fact that Cl has low surface sensitivity, which raised difficulties in deducing the Cl/Au ratio precisely. However, the EXAFS study of Au(I)/NaY-M indicated that the terminal Au–Cl coordination number (CN) was diminished and the total Au–Cl CN decreased to almost half that in Au_2Cl_6 reference sample, i.e., from 4 to 1.72 (21). After the CO chemisorption, the Cl/Au ratio increased to 1.28. This may be explained by the fact that the dissociative Cl atoms in AuCl(CO) were adsorbed on the surface rather than desorbed, where a large amount of free Cl species (perhaps as HCl) was detected by XPS. The TPD results supported this conclusion since HCl desorbed at temperatures higher than 373 K (Fig. 1).

FT-IR Study of OH Absorption Bands

The infrared spectra in the hydroxyl stretching region of NaY zeolite before and after Au_2Cl_6 loading at increasing temperatures are shown in Fig. 3. After 30 min evacuation of the samples at 400 K, distinct hydroxyl groups of zeolite became visible at frequencies of 3695, 3640, 3609, and 3523 cm^{-1}. The assignment of these peaks has already been reported (22–24). The brief evacuation of the sample at 400 K did not allow the reportedly weak band at about 3737 cm^{-1}, corresponding to the terminal SiOH groups, to be seen for any of the samples except Au_2Cl_6/NaY. Our attention will be focused on three peaks, namely those at 3695, 3640, and 3523 cm^{-1}, which showed the main IR spectral changes. The band at 3695 cm^{-1} in the spectrum of NaY zeolite is dramatically affected by Au_2Cl_6 loading and is virtually lost after mixing at room temperature. It was expected to disappear after the Au_2Cl_6/NaY reaction was conducted at temperatures higher than room temperature. According to this result one may think that this peak is probably not due to AlOH as previously suggested (25, 26), but is due to the cation–water interaction (27). However, Ward (23) did not rule out this peak for the rare earth-exchanged Y zeolite. On the contrary, the 3695 cm^{-1} peak was seen to grow with increasing fluorine loading on $SmCl_3$-exchanged NaY zeolite as reported by Kowalak *et al.* (28). They gave an uncertain assignment for this peak. However, the peak disappearance by the Au_2Cl_6 loading onto NaY zeolite suggests a strong interaction between Au_2Cl_6 and NaY zeolite even at room temperature. Further insight into this peak is given below.

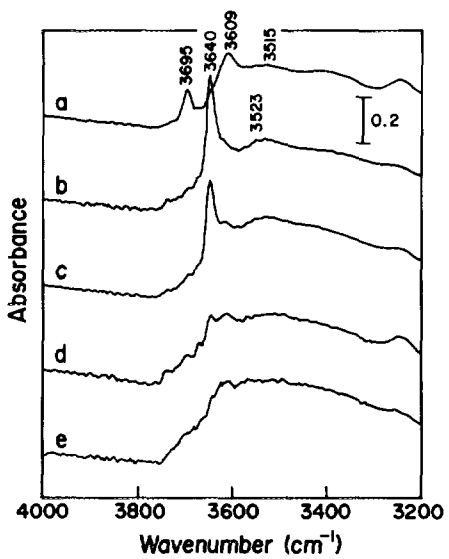

FIG. 3. FT-IR spectra of the hydroxyl region of samples dehydrated at 400 K for 30 min. (a) NaY, (b) Au_2Cl_6/NaY, (c) Au(I)/NaY-L, (d) Au(I)/NaY-M, and (e) Au(I)/NaY-H.

On the other hand, the added Au_2Cl_6 created a hydroxyl band at 3640 cm^{-1} stronger than that in unpromoted NaY, along with a very broad and ill-defined peak at 3523 cm^{-1}. A similar observation was reported for rare earth Y zeolite (23, 24). These OH bands systemically decreased in intensity and then vanished with raising Au_2Cl_6/NaY reaction temperature (Fig. 3e). It is highly feasible that the 3640 cm^{-1} observed peak for Au_2Cl_6/NaY, which is stronger than that for Au(I)/NaY-M, is associated with the Au^{n+} ($n > 1$) ions. Another conclusion that must be drawn from this observation is that $AuCl_n$ species did not react to displace silanol protons in SiOHAl structure but rather polarized H_2O in zeolite since the promoted gold species created new OH groups. We emphasize that the reaction between $AuCl_n$ species and water in zeolite is a typical low-temperature reaction. However, Ward (23) has carried out electrostatic field calculations for alkali, alkaline earth, and rare earth (RE) Y zeolite and concluded that the electrostatic field associated with the cation creates new OH band(s) (23, 24). Hence, the 3640 cm^{-1} band is probably accounted for by the Au^{n+} ($n > 1$) cation hydrolysis with vicinity H_2O in zeolite to produce a new OH peak. This leads to the justification of the peak at 3695 cm^{-1} by assuming that it is due to the cation–H_2O interaction in bare zeolite. The complete reduction of the 3695 cm^{-1} peak intensity upon Au_2Cl_6 introduction together with the formation of new hydroxyl groups at 3640 cm^{-1}

suggests that the adsorbed water in zeolite undergoes reaction according to

$$AuCl_3 + H_2O\text{–}Z \rightarrow AuCl_2 + OH\text{–}Z + HCl \quad [2]$$

$$AuCl_2 + H_2O\text{–}Z \rightarrow AuCl + OH\text{–}Z + HCl, \quad [3]$$

where OH–Z is a hydroxyl group-attached NaY zeolite and nearby regions of Au^{n+} ($n > 1$) ions. The broad band at about 3523 cm^{-1} is likely due to OH associated with Au^{n+} ($n > 1$) species. This band has been previously assigned to REOH groups (23). A charge transfer from polarized OH^- to Au(III) is possibly accounted for by its reduction to Au(I) (24).

The simultaneous decrease in the 3640-cm^{-1} band intensity with increasing temperature can be explained as follows: The multivalent Au(III) cations were reduced to a lower oxidation state(s) as indicated from the XPS results, thereby causing the electrostatic potential field associated with Au^0 and/or Au^{n+} ($n < 3$) to become insufficient to polarize H_2O into H^+ and OH^-. The peak at 3695 cm^{-1} was not expected to be reproduced again in these circumstances because the reduction of Au(III) ions by adsorbed H_2O was accelerated and new OH groups could appear/disappear throughout the process. The XRD data revealed that the relatively high temperatures employed for the catalyst preparation, i.e., 353 K, resulted in the segregation of Au metallic phase. From the foregoing explanations, the intensity of the 3640 cm^{-1} band can be taken as a measure of the amount of Au(III).

Effect of H_2O Adsorption on the 3640 cm^{-1} Peak Intensity

Figure 4 shows the effect of water as a function of 3640-cm^{-1} peak intensity. Upon the addition of a small amount

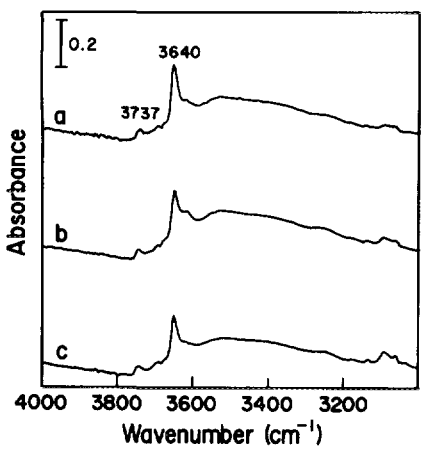

FIG. 4. FT-IR spectra of hydroxyl groups in Au_2Cl_6/NaY. The sample was (a) evacuated for 30 min at 400 K, (b) exposed to 10 μmol H_2O at 295 K followed by evacuation at 373 K, and then (c) evacuated at 400 K.

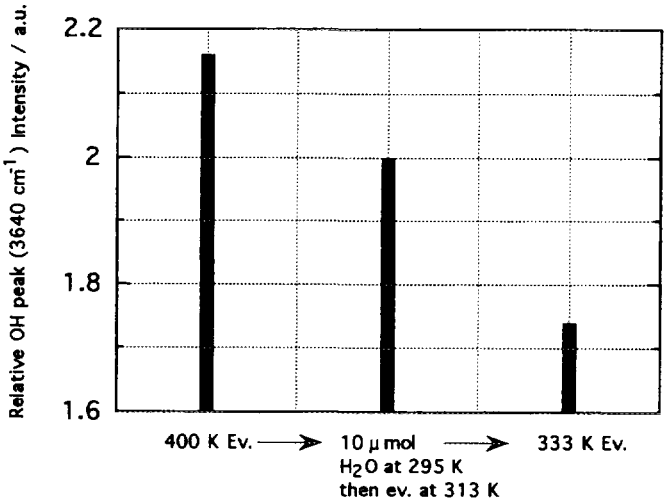

FIG. 5. Effect of adsorbed H_2O on the 3640 cm^{-1} peak intensity of Au_2Cl_6 in sequential (successive) treatment.

of H_2O (10 μmol) at room temperature onto the Au_2Cl_6/NaY sample dehydrated at 400 K, followed by the evacuation at 373 K (Fig. 4b), no additional hydroxyl groups were observed. Similar results were obtained for adsorbed H_2O on rare earth cations in zeolites (23). The 3640 cm^{-1} band decreased in intensity after H_2O adsorption, although the evacuation temperature was lower than that used in an earlier step. The increase in the evacuation temperature to 400 K resulted in a further decrease in peak intensity as shown in Fig. 5. It is likely that such a decrease in peak intensity is caused by the reduction of some Au(III) cations by the aid of H_2O in zeolite to a lower oxidation state(s).

FT-IR Study of OD-Exchanged OH Groups

To draw a firm conclusion regarding the role of H_2O in the reduction of Au(III) ions, the changes in the OH band frequencies by the systematic increase in the Au_2Cl_6/NaY reaction temperature are shown in Fig. 6. The corresponding spectra of exchange of surface hydroxyls with D_2O on NaY and Au_2Cl_6/NaY are shown in Fig. 7. The initial spectrum of Au_2Cl_6/NaY after the evacuation at 313 K has two OH bands at 3640 and 3525 cm^{-1}. When the reaction temperature was increased by the evacuation at 333 K, the latter band was shifted to the higher frequency side, i.e., 3550 cm^{-1}. Increasing the evacuation temperature to 400 K led to an overall broad peak similar to that observed around 3523 cm^{-1} in Fig. 3. This broad peak may arise due to the transition in oxidation states of gold species at this temperature. It is worth noting that the peak at 3640 cm^{-1} did not decline to an appreciable extent even after evacuation of the Au_2Cl_6/NaY sample at 400 K. This is because a long reaction time between Au_2Cl_6 and

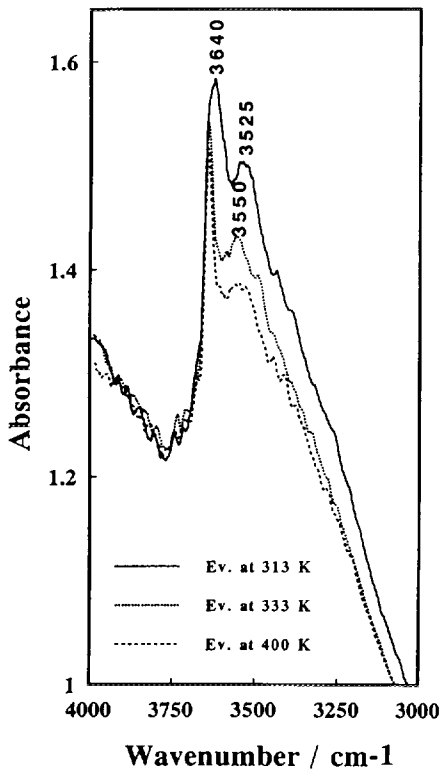

FIG. 6. FT-IR spectra of hydroxyl groups in Au_2Cl_6/NaY after dehydration at increasing temperatures.

partially dehydrated zeolite is needed to accommodate $AuCl_n$ species into zeolite. The $AuCl_n$ species is activated in pores of NaY zeolite as will be shown later.

Adsorption of D_2O at 295 K on unpromoted NaY zeolite produced a sharp peak at 2732 cm^{-1} due to the O–D stretching vibration in Si–OD moiety (Fig. 7a). The same band was developed in the spectrum of Au_2Cl_6/NaY under the same conditions (Fig. 7b). The hydroxyl groups on unpromoted and promoted NaY zeolite which produced an absorption band at 3640 cm^{-1} were replaced by deuteroxyl groups, giving rise to a corresponding band at 2732 cm^{-1}. It is quite evident now that ultimately the hydroxyl groups at 3640 cm^{-1} were associated with NaY support and not with Au^{n+} species, in agreement with Eqs. [2] and [3]. Besides, a peak was observed at 2656 cm^{-1} in the spectrum of Au_2Cl_6/NaY. This peak did not arise in the spectrum of NaY. Therefore, this band is assigned to OD groups attached on Au^{n+} ($n > 1$) due to the exchanged OH groups at 3525 cm^{-1} (Fig. 6). The 2656-cm^{-1} frequency differs by a factor of 1.33 from the corresponding OH stretching frequency.

When D_2O was evacuated at 313 K, the OD bands were progressively removed except for that attached to Au^{n+} ($n > 1$) at 2656 cm^{-1} (Fig. 7c). On the other hand, a newly generated shoulder at 2690 cm^{-1} was observed. Further evacuation of D_2O at 333 K diminished the peak at 2656 cm^{-1} in favor of a peak at 2690 cm^{-1} (Fig. 7d). The latter peak is assigned to O–D stretching vibration in the Au(OD)Cl moiety of the exchanged OH band at 3550 cm^{-1} (Fig. 6). The 2690 cm^{-1} frequency differs by a factor of 1.33 from the corresponding OH frequency. This leads to the conclusion that the OH bands at 3525 and 3550 cm^{-1} are associated with Au(III) and Au(I), respectively. As a result of D_2O thermal evacuation, the Au^{n+} ($n > 1$) cations were reduced into Au(I) in the same way as discussed above. The XPS data showed that the Au(I)/NaY-M sample, which was prepared by the evacuation of Au_2Cl_6/NaY at the same D_2O evacuation temperature, contained the higher surface concentration of Au(I). It is reasonable for the OD band characteristic of Au(I) to be located at a wavenumber higher than that of $Au^{n+}OD$ ($n > 1$) since the cation radius of Au(I) is smaller than that of Au^{n+} ($n > 1$). It is interesting to observe that the Au(I)OD band is more stable than the other OD bands upon thermal evacuation.

FT-IR Study of CO Chemisorption at 77 K

Figure 8 shows the FT-IR results of the *in situ* interaction of 0.5 Torr CO with NaY and Au(I)/NaY-M at 77 K. A sole peak is observed for CO adsorbed onto NaY zeolite (Fig. 8b). On the other hand, two main peaks at 2188 and 2176 cm^{-1} and a very small one at 2120 cm^{-1} were observed in the spectrum of CO adsorbed onto Au(I)/NaY-M after 5 min exposure time (Fig. 8b). By increasing the interaction time, the band at 2188 cm^{-1} was built up slowly at the expense of the band at 2176 cm^{-1}. The former

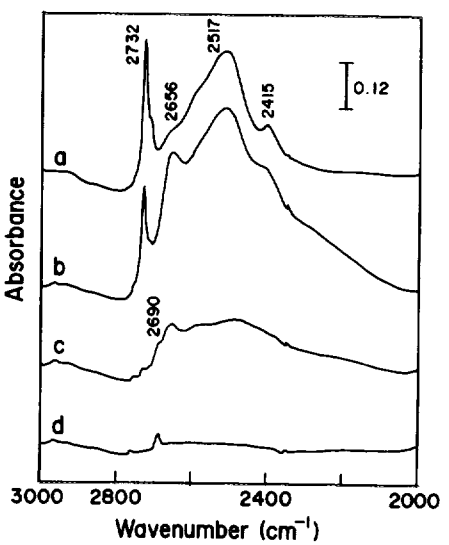

FIG. 7. FT-IR spectra of surface deuteroxyl groups attached on (a) NaY after D_2O evacuation at 295 K and on Au_2Cl_6/NaY after D_2O evacuation at (b) 295 K, (c) 313 K, and (d) 333 K.

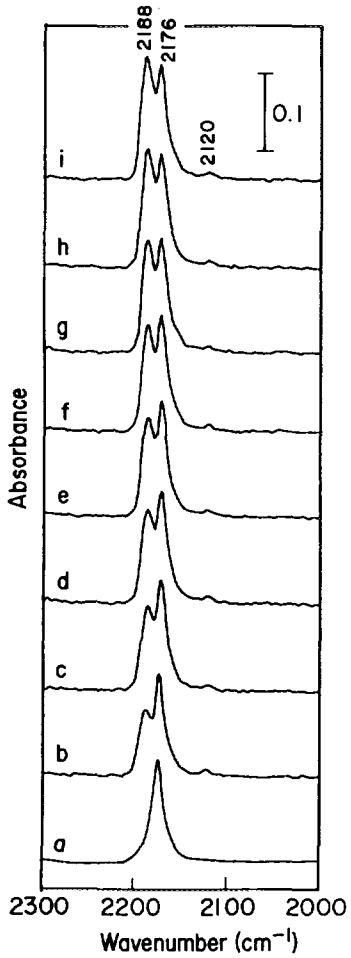

FIG. 8. *In situ* FT-IR spectra of CO (0.5 Torr) adsorbed at 77 K on (a) unpromoted NaY and on Au(I)/NaY-M for (b) 5 min, (c) 10 min, (d) 20 min, (e) 30 min, (f) 40 min, (g) 1 h, (h) 1.5 h, and (i) 2 h.

band ascribed to C≡O stretching frequency of CO species chemisorbed to the Au cationic site (29). This assignment comes from a peak shift to frequencies higher than that of free CO at 2155 cm^{-1}. It was reported that CO coordinating to Au(I) in Au/W (29) and to Ag(I) in AgX (30) appeared at about 2176 cm^{-1}. However, the XPS and IR of D_2O adsorption results demonstrated that the Au(I) ions prevail in the Au(I)/NaY-M sample. The high frequency shift of the CO band (ca. 12 cm^{-1}) relative to that previously reported for CO → Au(I)/W is interpreted in terms of C- and O-ended CO interaction of Au(I)CO with acidic Al^{3+} and H^+ sites in the zeolite cages.

The 2176-cm^{-1} band is due to CO gas phase condensed in the cages of zeolite. Although this frequency coincided with that reported for CO → Au(I)/W, there are increasing facts supporting our assignment. First, this stretching CO band was obtained with bare NaY zeolite (Fig. 8a). Second, the peak diminished by reducing the CO pressure, as is shown later. Third, it did not develop at room temperature for the same catalyst (8). In addition, the peak is formed instantaneously after the CO admittance and shows no remarkable changes when the contact time is increased. The negligible small peak at 2120 cm^{-1} is attributed to CO species adsorbed on Au metal (7). It must be mentioned that no other CO peaks were detected, unlike in a work by Miessner *et al.* (31), where the authors observed additional broader bands with CO interacted with $Rh(I)(CO)_2$/NaY. These bands were located at 2090 and 2040 cm^{-1} and assigned to carbonyl species on the outer surface of zeolite.

The reduction of the CO pressure after adsorption for 2 h at 77 K led to a simultaneous decrease and then disappearance of the peak at 2176 cm^{-1} (Fig. 9). The very small hump at 2120 cm^{-1} disappeared very quickly. This indicates that CO adsorbed very weakly on gold surface (9). Meanwhile, the peak at 2188 cm^{-1} is preserved to support its dependence on the stability of the Au(I) structure. It follows that Au(I)/NaY-M contains a substantial amount of Au(I) centers with a small fraction close to Au^0. The integrated peak area of 2188 cm^{-1} is 39 times larger than that of 2120 cm^{-1}. We can, however, conclude from this that the number of Au(I) ions accessible to CO (i.e., located in the supercages) is 97.5% of the total Au content, assuming homogeneous distribution of Au spe-

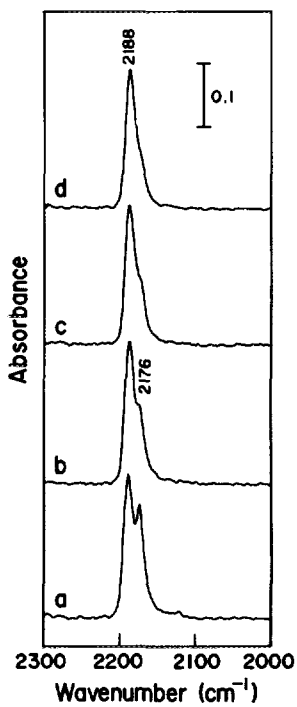

FIG. 9. *In situ* FT-IR spectra recorded at reduced CO pressures on Au(I)/NaY-M (a) at 0.5 Torr adsorption for 2 h, (b) after it was evacuated to 0.25 Torr, (c) after it was evacuated to 0.1 Torr, and (d) after it was evacuated to 0.01 Torr.

cies. Unlike Ag(I) in zeolite, which forms $[Ag_3]^{n+}$ clusters (32), the Au(I) ions formed with a stable monoatomic structure by interaction with zeolite, although a large amount of Au_2Cl_6 was incorporated. The unique carbonyl peak at 2188 cm^{-1} undoubtedly indicates that the Au(I) ions in NaY zeolite are in good configuration.

FT-IR Study of Pyridine and Chlorine Adsorptions

In order to evaluate the fate of protons generated during the interaction of Au_2Cl_6 with partially dehydrated zeolite, FT-IR spectra of pyridine adsorption were obtained (Fig. 10). The assignment of the spectra peaks has been given by Parry (33). It is clearly shown that the amount of Brønsted acid sites at 1558 cm^{-1} increased as the reaction temperature of Au_2Cl_6–NaY increased from 338 to 353 K. Although new OH groups at 3640 cm^{-1} which are acidic in nature were generated during the reaction, the contribution of HCl protons in producing Brønsted acid sites is greater. This conclusion is confirmed by the IR spectrum of Au(I)/NaY-H, which did not display the 3640-cm^{-1} band. On the other hand, the amount of Lewis acid sites at 1442 cm^{-1} decreased in the same sequence. Such a decrease is presumably caused by the chlorine or HCl coordination to aluminum.

Kwak and Sachtler have studied the acidic properties of $GaCl_3$/HZSM-5 prepared by the CVD method in connection with C_3 conversion to aromatics (34). In contrast to our results, introduction of Ga lowered the Brønsted acidity, but introduced new Lewis acid sites into the catalyst. However, their catalyst preparation method allowed proton replacement of OH-zeolite by Ga during the $GaCl_3$/ZSM-5 (pre-evacuated at 773 K) reaction at elevated temperature, i.e., 773 K. They claimed that HCl is removed

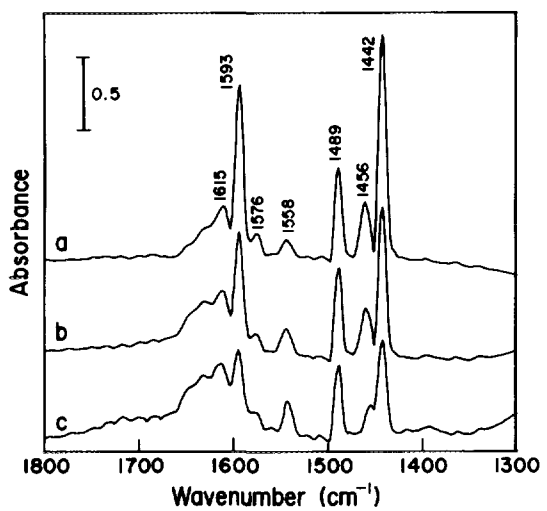

FIG. 10. FT-IR spectra of pyridine (2 Torr) adsorption on (a) Au(I)/NaY-L, (b) Au(I)/NaY-M, and (c) Au(I)/NaY-H.

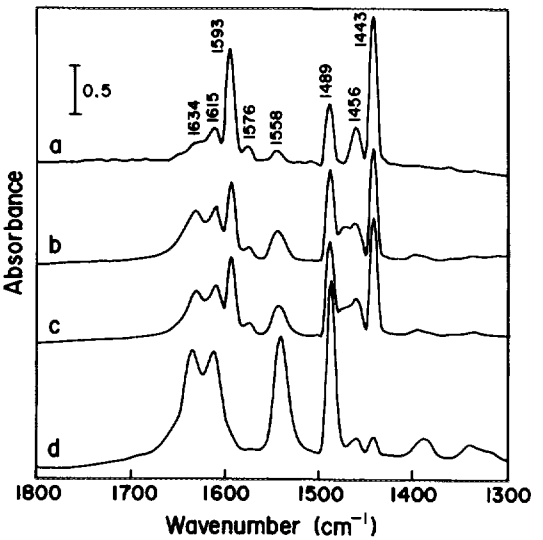

FIG. 11. FT-IR spectra of Au(I)/NaY-L after successive pyridine–Cl adsorptions at 295 K followed by the evacuation at the same temperature (a) after pyridine adsorption, (b) after (a) Cl_2 was adsorbed for 5 min, (c) after (b) pyridine was adsorbed, and (d) after (c) Cl_2 was adsorbed for a prolonged time (30 min).

at the reaction temperature. Our TPD results showed that HCl is firmly adsorbed into the gold catalyst and was not removed even at temperatures as high as 773 K. It seems then that Brønsted acidity is influenced not mainly by the catalyst preparation conditions, but by the entire structure of the zeolite. The dominance of Al^{3+} ions in NaY rather than in ZSM-5 led to the stabilization of HCl.

To study the effect of Cl atom removal through the $AuCl_3$ reduction process on the generation of Brønsted acid sites in Au(I)/NaY-L, Fig. 11 shows the FT-IR spectra of pyridine–Cl_2 adsorptions after 5 min. When pyridine followed by Cl_2 was adsorbed the Brønsted acidity was enhanced at the expense of Lewis acidity as shown from the peak intensity increases at 1558 and 1634 cm^{-1}. Subsequent pyridine adsorption did not change the spectrum, suggesting that the Au(I) ions in NaY zeolite are stable toward oxidation by Cl_2. Following this, Cl_2 was admitted for a prolonged time (30 min) to yield a spectrum (Fig. 11d) which indicates the existence of only Brønsted acid sites. It is reported (35) that AuCl forms *L*AuCl structure, where *L* is a ligand, e.g., pyridine, but it seems that the protons in HCl compete strongly for pyridine.

Kim *et al.* (36) studied the crystal structure of a chlorine sorption complex of partially dehydrated fully Ag^+-exchanged zeolite A by single-crystal X-ray diffraction. They found the Cl–Cl bond length, 2.49 Å, to be considerably longer than that of free Cl_2 (1.99 Å). They suggested that H^+ bridges between two chlorine molecules and electron-pair donation (charge transfer) take place between

the electronegative O(I) and the chlorine molecules. This is manifested by the elongated dichlorine bond length that the chlorine molecule activated in pores of zeolite. This is why Cl_2 was not observed by TPD for the thermal Au_2Cl_6/NaY reaction and instead the feasible formation of Brønsted acidity was observed. Electronic structure investigation of Au(I)/NaY-M and -L samples by UV–vis spectroscopy showed four bands in the high-energy side of their spectra (20). Two were reported for the Cl (terminal and bridge) → Au charge transfer in Au_2Cl_6, while the other two were not reported (37). The Cl (terminal) → Au band vanished for Au(I)/NaY-H and the other peaks underwent broadening. Most probably, such broadening is due to the mutual interaction between Au_2Cl_6 and NaY zeolite. The disappearance of the Cl (terminal) → Au band is supported by the XPS and EXAFS data. The XRD analysis indeed indicated that the Au phase grew in Au(I)/NaY-H. The decrease in the Lewis acidity with an increase of the catalyst preparation temperature may dictate that the two unassigned peaks are due to the Cl → Al charge transfer. Further study is needed to confirm this assignment.

CONCLUSIONS

Solid–vapor reaction at ambient temperatures has been proven to be an efficient method for producing large amounts of active Au(I) ions in partially dehydrated zeolite. H_2O was found to play a vital role in the reduction of Au(III) into Au(I) ions. A strong OH band at 3640 cm^{-1} characteristic of Au^{n+} ($n > 1$) was detected by FR-IR. By the D_2O adsorption on Au_2Cl_6/NaY at room temperature followed by the desorption at 333 K, a new stretching OD band was produced at 2690 cm^{-1} which is believed to be due to the presence of Au(OD)Cl moiety. The XPS investigation supported this assignment, where the catalyst prepared under the same conditions contained merely AuCl species. The HCl released during the Au_2Cl_6–H_2O reaction in zeolite enhanced the Brønsted acidity of the catalyst. Subsequent pyridine–chlorine adsorption onto the Au(I)/NaY catalyst showed that the Au(I) ions are stable toward oxidation by Cl_2 since no enhancement in the Lewis acidity was observed. Exposure of Au(I)/NaY to Cl_2 for a prolonged time led to a complete exchange of Lewis by Brønsted acid sites, indicating that the Cl atoms were activated in pores of zeolite. CO chemisorption at 77 K onto Au(I)/NaY revealed that Au(I) ions prevail in the catalyst prepared at 338 K. The introduction of coordinatively unsaturated Au(I) center into NaY zeolite enhanced the ability of the catalyst to adsorb CO. According to this observation, one must consider the catalysis by gold from the viewpoint of charged Au species rather than Au metal as the active sites.

ACKNOWLEDGMENTS

The authors gratefully thank Dr. R. Ohnishi for useful discussions and Dr. H. Ohtani for reading the manuscript.

REFERENCES

1. Cant, N. W., and Hall, W. K., *J. Phys. Chem.* **75,** 2914 (1971).
2. Galvagno, S., and Parravano, G., *J. Catal.* **55,** 178 (1978).
3. Schwank, J., Parravano, G., and Gruber, H. L., *J. Catal.* **61,** 19 (1980).
4. Shastri, A. G., Datye, A. K., and Schwank, J., *J. Catal.* **87,** 265 (1984).
5. Haruta, M., Kobayashi, T., Sano, H., and Yamada, N., *Chem. Lett.*, 405 (1987).
6. Karge, H. G., and Beyer, H. K., *Stud. Surf. Sci. Catal.* **69,** 43 (1991).
7. Ozin, G. A., *Acc. Chem. Res.* **10,** 21 (1977).
8. Qiu, S., Ohnishi, R., and Ichikawa, M., *J. Chem. Soc. Chem. Commun.*, 1425 (1992).
9. Qiu, S., Ohnishi, R., and Ichikawa, M., *J. Phys. Chem.* **98,** 2719 (1994).
10. Salama, T. M., Qiu, S., Ohnishi, R., and Ichikawa, M., *Shokubai* **36,** 80 (1994).
11. Minagawa, H., Vina, P. O., Kadowaki, T., Mizuno, S., Tochihara, H., Hayakawa, K., and Toyoshima, I., *Jpn. J. Appl. Phys.* **31,** L1709 (1992).
12. Briggs, D., and Seah, M. P., "Practical Surface Analysis, Vol. 1, Auger and X-Ray Photoelectron Spectroscopy," John Wiley & Sons, 2nd ed., 1990.
13. Kishi, K., and Ikeda, S., *J. Phys. Chem.* **78,** 107 (1974).
14. Kharasch, M. S., and Isbell, H. S., *J. Am. Chem. Soc.* **52,** 2919 (1930).
15. Dell'Amico, D. B., and Caderazzo, F., *Gazz. Chim. Ital.* **103,** 1099 (1973).
16. Janssen, E. M. W., Pohlmann, F., and Wiegers, G. A., *J. Less Common Met.* **45,** 261 (1976).
17. Janssen, E. M. W., Folmer, J. C. W., and Wiegers, G. A., *J. Less Common Met.* **38,** 71 (1974).
18. Koley, P. A., Nirmala, R., Prasad, L. S., Ghosh, S., and Manoharan, P. T., *Inorg. Chem.* **31,** 1764 (1992).
19. Janssen, E. M. W., Folmer, J. C. W., and Wiegers, G. A., *J. Less Common Met.* **38,** 71 (1974).
20. Straehle, J., and Loercher, K. P., *Z. Naturforsch. B* **29,** 266 (1974).
21. Salama, T. M., Shido, T., and Ichikawa, M., in preparation.
22. Rabo, J. A., Angell, C. L., Kasai, P. H., and Schomaker, V., *Discuss. Faraday Soc.* **41,** 328 (1960).
23. Ward, J. W., *J. Phys. Chem.* **72,** 4211 (1968).
24. Ward, J. W., *J. Catal.* **13,** 321 (1969).
25. Angell, C. L., and Schaffer, P. C., *J. Phys. Chem.* **69,** 3463 (1965).
26. Ward, J. A., *J. Catal.* **9,** 225 (1967).
27. Olson, D. H., *J. Phys. Chem.* **72,** 1400 (1968).
28. Kowalak, S., Laniecki, M., Khanmamedova, A. K., and Balkus, K. J., Jr., *Catal. Lett.* **24,** 257 (1994).
29. Huber, H., McIntosh, D., and Ozin, G. A., *Inorg. Chem.* **16,** 976 (1977).
30. Gellens, L. R., Mortier, W. J., Schoonheydt, R. A., and Uytterhoeven, J. B., *J. Phys. Chem.* **85,** 2783 (1981).
31. Miessner, H., Burkhardt, I., Gutschick, D., Zecchina, A., Morterra, C., and Spoto, G., *J. Chem. Soc. Faraday Trans.* **86,** 2321 (1990).
32. Jacobs, P. A., Uytterhoeven, J. P., and Beyer, H., *J. Chem. Soc. Faraday Trans. 1* **75,** 56 (1979).
33. Parry, E. P., *J. Catal.* **2,** 371 (1963).
34. Kwak, B. S., and Sachtler, W. M. H., *J. Catal.* **145,** 456 (1994).
35. Mundorf, V. T., and Dehnicke, K., *Z. Anorg. Allg. Chem.* **408,** 146 (1974).
36. Kim, Y., and Seff, K., *J. Am. Chem. Soc.* **100,** 3801 (1978).
37. Nalbandian, L., Boghosian, S., and Papatheodorou, G. N., *Inorg. Chem.* **31,** 1769 (1992).